Letters in Applied NanoBioScience
Open-Access Journal (ISSN: 2284-6808)

Article
Volume 13, Issue 4, 2024, 200
https://doi.org/10.33263/LIANBS134.200

CoMFA and CoMSIA Study of CD4-mimetic Small Molecules as HIV-1 Entry Antiviral Inhibitors

Farid Elbamtari [1,*], Mhamed Elbouhi [1], Allal Fakkahi [1], Kamal Tabti [1], M'barek Choukrad [1], Tahar Lakhlifi [1], Mohammed Bouachrine [1,2]

[1] Molecular Chemistry and Natural Substances Laboratory, Moulay Ismail University, Faculty of Sciences, Meknes, Morocco; faridelbamtari@gmail.com (F.E.); mhamed.elbouhi@usmba.ac.ma (M.E.); fakkahiallal18@gmail.com (A.F.); k.tabti@edu.umi.ac.ma (K.T.); mchoukrad@yahoo.fr (M.C.); tahar.lakhlifi@yahoo.fr (T.L.);
[2] Higher School of Technology – Khenifra (EST Khenifra), Sultan Moulay Sliman University, PB170, Khenifra 54000, Benimellal, Morocco; bouachrine@gmail.com (M.B.);
* Correspondence: faridelbamtari@gmail.com (F.E.);

Scopus Author ID N.A.

Received: 1.05.2023; Accepted: 11.08.2023; Published: 28.08.2024

Abstract: Studies conducted on the chain include nitrobenzoxadiazole (NBD) against HIV-1HXB2, based on comparative CoMFA and CoMSIA interpretations that consider quantitative structure-activity relationship analyses. The CoMFA type sees that the electrostatic and steric fields for the confirmed value of the learning set Q^2 are equal to 0.625 with an estimate of R^2 that equals 0.996 and SEE=0.043. Also, for the CoMSIA type, the value found for Q^2 is 0.631, and a practically unvalidated evaluation value of R^2 is 0.738, and SEE=0.298. This means that of all the inhibitors examined, the only one that shows high antiviral resistance against HIV-1HXB2 is NBD-14246 (S) and a high selection factor compared to various compounds.

Keywords: QSAR; nitrobenzoxadiazole (NBD); HIV-1HXB2; CoMFA; CoMSIA.

1. Introduction

Infection with HIV-1 leads to a major global health risk that results in symptoms of acquired immunodeficiency [1]. Treatment by highly active antiretroviral therapy (HAART), which combines various reverse transcriptase and protease inhibitors to temporarily block viral development, makes it possible to accomplish this goal. The toxicity of HAART limits its use in anti-HIV therapy today. On the other hand, the biological functioning of these agents is confined to the continuous appearance of new viral-resistant strains [2]. Therefore, the development of novel, effective antiretroviral medications is still desired. According to the latest studies and statistics in 2019, they obtained 38 million of the world's population has been impacted by HIV [3]. When the outbreak first started, a staggering 76 million people had this fatal illness, and 32 million of them passed away from it 25.4 million have received antiretroviral treatment, and about 690,000 have died of diseases associated with acquired immunodeficiency syndrome [4]. HIV is a protected infectious RNA single-stranded virus with a beneficial effect that is part of the breed retrovirus and the genus Lentivirus. Antiretroviral medicines (ARVs) have been used for HIV-1 infection is a remedy with this medication because there is currently no cure [5,6]. Extremely effective antiviral treatment (HAART) permits the reconstitution of CD4+ T-cell populations while suppressing virus replication in plasma to practically undetectable levels. Two or more classes of ARVs, each of which targets

a different stage of the HIV-1 period of life, make up a typical HAART regimen [7]. Today, the four licensed forms of antiretroviral drug treatment for HIV-1 are integrase inhibitors 6, protease inhibitors, entry inhibitors, and reverse transcriptase inhibitors (RTIs); even if this success is unexpected, there are various restrictions with existing treatments [8]. For example, relying on daily commitment, long-term toxicity caused by prolonged use, reduced therapy choices brought on by the development of medication resistance, high price, and ineffectiveness of current drugs [9–11]. Therefore, there is further development of highly potent small molecule drugs against this. The need for fewer side effects and new targets is essential. The creation of new treatments will contribute to the availability of a significant number of new medicines, and the expansion of the spectrum of combination medicines association and fusion of the virus with the host cell membrane is essential for HIV-1 to enter the host cell and utilize its mechanisms [12,13]. As the virus begins its life cycle (often referred to collectively as "viral entry") it determines the destination for creating a new drug.

The present study shows that compounds with nitrobenzoxadiazole (NBD) backbones have significant useful properties such as environmental sensitivity [14]. It has high reactivity towards amines and biothiols (including H_2S), significant color and fluorescence changes, fluorescence quenching capability, and a small size that facilitates biomolecular detection and product discrimination. Amines are crucial biological nucleophiles, and NBD ethers' special interaction with amines has made it possible to label proteins and detect enzymatic activity [15,16] specifically. In mammals, biothiols and H_2S are involved in various physiological processes, and their improper control is linked to several illnesses, including cancer. A 3D-QSAR investigation was carried out; it is one of the greatest techniques for anticipating chemical compounds' biological effects based on mathematical and statistical correlations. Additionally, it incorporates and enhances research on how drugs and chemicals work [17]. We employ CoMFA and CoMSIA molecular field comparison analysis methods for this aim, which are productively applied in drug discovery development [18]. The key objective of our research is to build a predictive model that has been successfully used in drug design and to explain the connection between the molecular characteristics and biological processes of HIV-1 entry inhibitors [19].

2. Materials and Methods

2.1. Data sources.

The existing 3D-QSAR testing used a dataset of 32 HIV-1 NBD series CD4 small molecule mimics reported to affect HIV-1 infection in CD4-CCR5+ cells [20]. Replication (CoMFA and CoMSIA). The inhibitory concentration IC_{50} (μM) of each molecule was adapted to pIC_{50}(M) as indicated in table 1. The SYBYL program has been adopted by default. The Gasteiger-Huckel method was used to compute the partial atomic charge, and the kind tripos force field was used to accomplish minimizations. The built molecules were placed on the docked conformation of NBD compounds to generate the 3D-QSAR models' requirement for molecular spatial alignment.

Table 1. NBD compounds anti-HIV-1 activity (pIC_{50}) against HIV-1 HXB2 in a single-cycle experiment.

N	Structure	pIC_{50}
1*	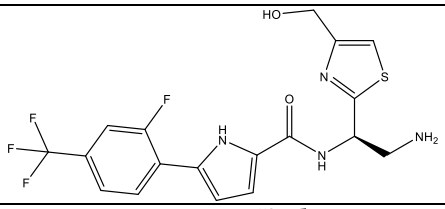	6.215
2	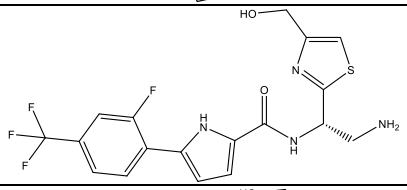	6.728
3*	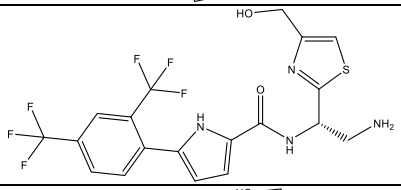	5.377
4	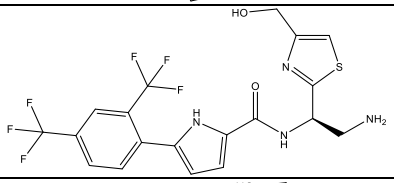	5.201
5	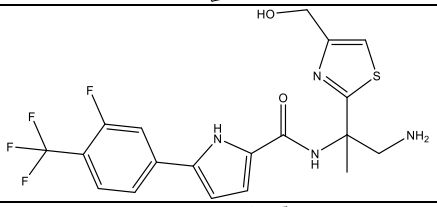	5.796
6*	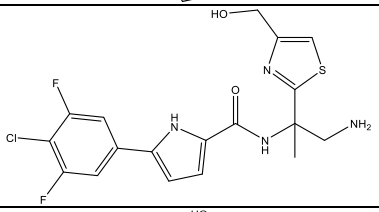	5.585
7	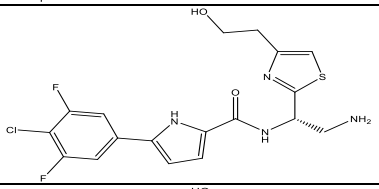	6.824
8	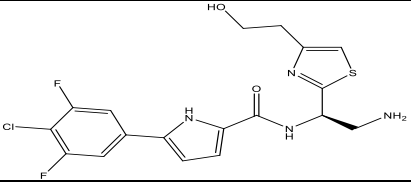	6.009
9*	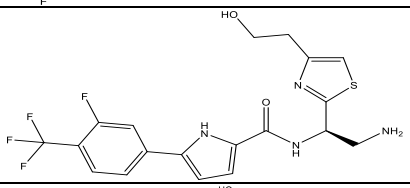	6.292
10	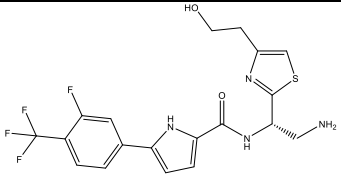	6.699

N	Structure	pIC_{50}
11	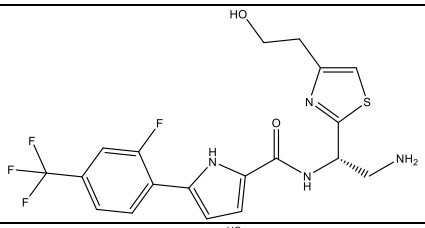	6.745
12*	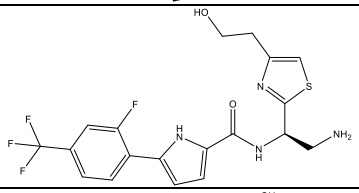	6.824
13	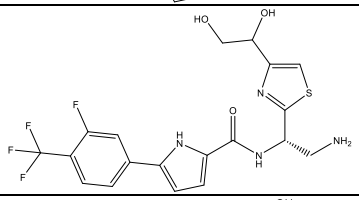	6.260
14	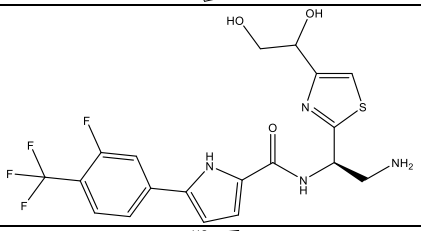	5.620
15	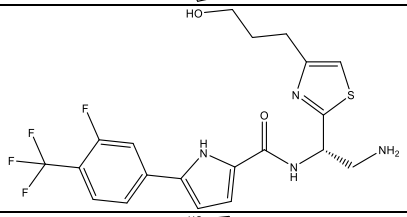	6.602
16	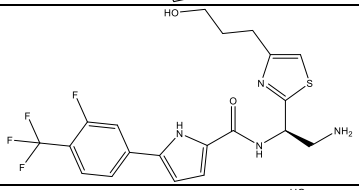	5.456
17*	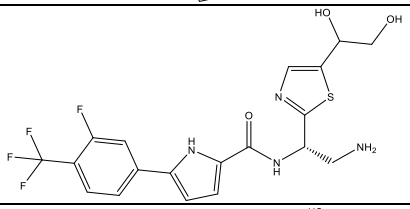	5.208
18*	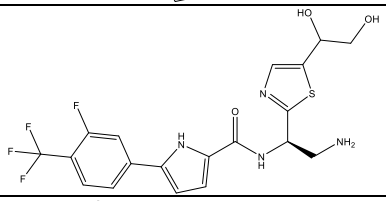	6.229
19	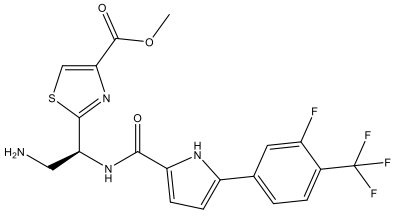	5.538

N	Structure	pIC_{50}
20	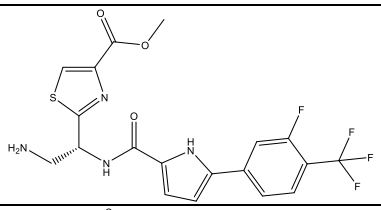	5.310
21*	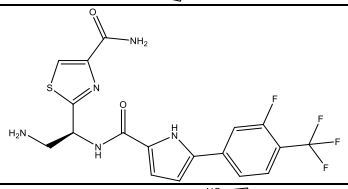	5.638
22	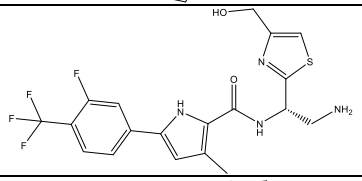	6.268
23	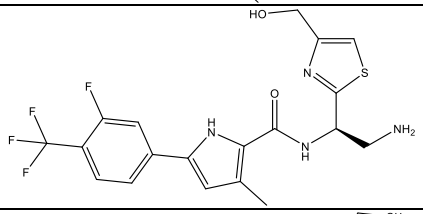	6.244
24	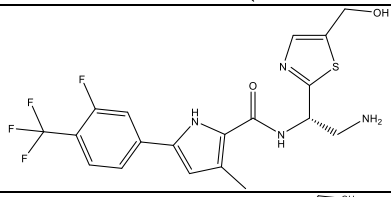	6.824
25	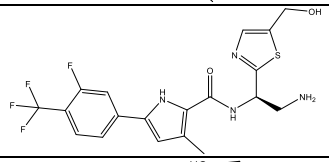	6.678
26*	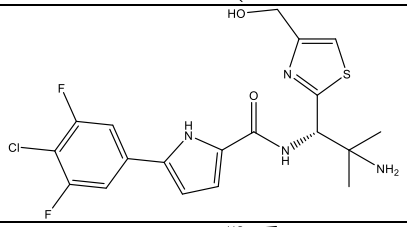	6.921
27	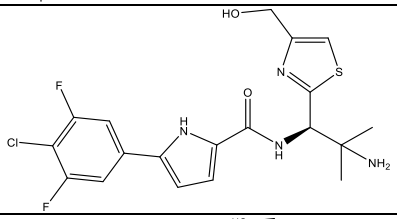	6.824
28	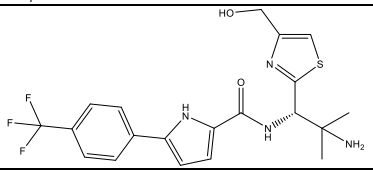	6.886
29	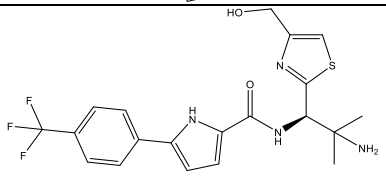	5.886

N	Structure	pIC_{50}
30	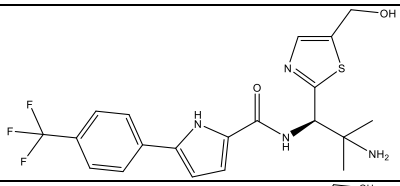	6.167
31	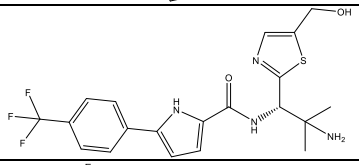	6.638
32	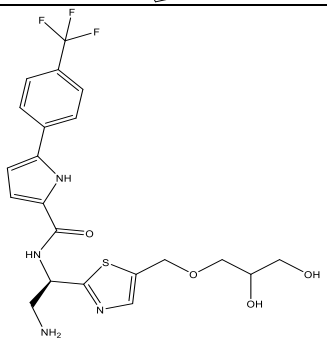	5.678

* test molecules

2.2. 3D-QSAR models.

The SYBYL-X software suite was used to create all calculations and molecular models using the ““SKETCH”” option service in SYBYL [21]. A base molecule was used to build the architectures of all inhibitors. Energy minimizations were carried out utilizing the Powell conjugate gradient decrease method and the tripos force field using a 0.01kcal/mol convergence limit [22]. The Gasteiger-Hückel charge is utilized to compute the partial atomic charges. The sizing of the electrostatic and steric domain in the CoMFA using SYBYL CoMFA-STD technique using the partial as to squares (PLS) methodology, a multiple regression analysis extension [23], CoMFA Q^2 values were obtained Based on the initial ideal number of components (ONC), and the cross-validated standard error of prediction was obtained using cross-validation of the Leave-One-Out method (LOO) choice [24]. In the end, the ideal proportion of components was used to create a cross-validated model, employing the same lattice box as CoMFA, and CoMSIA fields were produced. Steric, electrostatic, hydrophobic, hydrogen bond donor, and hydrogen bond acceptor are the five descriptors included in CoMSIA. According to the procedure outlined by Klebe et al., these descriptors, known as similarity indices, were calculated [25]. The five separate descriptor fields used in the CoMSIA analysis are not entirely independent. The values that were the most effective cross-validation Q2, the fewest mistakes, and the greatest F values were selected after systematically changing the field combinations to obtain the best result [26].

2.3. Molecular modeling alignment.

All calculations to find the model molecules were performed with the Sybyl software package due to its high power. Compound 31 was used as a model using the SYBYL-X optional “SKETCH” function; the model molecule served as the foundation from which all inhibitor constructions are built [27]. Powell's approach for minimizing conjugate gradients and Tripos force area was used for energy minimization with a matching threshold of 0.01kcal/(molÅ). To determine the partial atomic charges utilizing the Powell conjugate gradient minimization

approach and a 0.01kcal/(molÅ) convergence limit [28,29]. The Gasteiger-Hückel charge is utilized to compute the atomic charges that are partial database alignment functions of SYBYL-X data management software [30]. The figure shows that other training and test compounds will be modeled after compound 31, as shown in Figure 1.

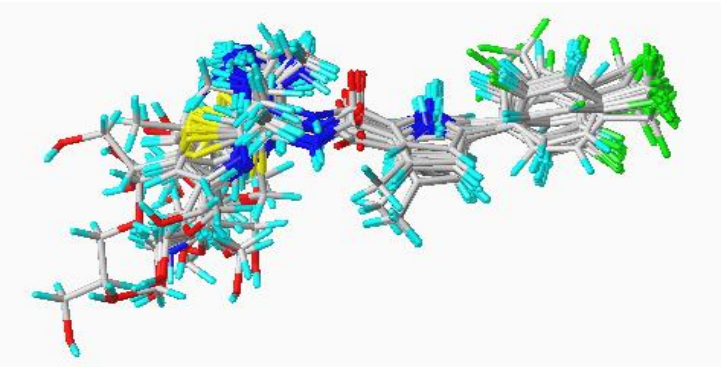

Figure 1. Demonstrates how the compounds are aligned.

3. Results and Discussion

3.1. Model CoMFA and CoMSIA model results.

In this work, we have developed a CoMFA model and CoMSIA models with different possible combinations of steric (S), electrostatic (E), hydrophobic (H), and hydrogen bond donor/acceptor (D/A) fields. The best models that show good statistical results are CoMFA and CoMSIA (SHD), as summarized in Table 2.

Table 2. Summary of the CoMFA and CoMSIA analysis results.

Statistical Variables	CoMFA model	CoMSIA/SHD model
Q^{2u}	0.625	0.631
R^{2v}	0.996	0.738
SEE ^{w}	0.043	0.298
F-value ^{x}	622.370	59.122
R^2_{TEST} ^{y}	0.786	0.823
ONC^{z}	6	1
Steric	0.575	0.254
Electrostatic	0.425	-
Hydrophobic	-	0.271
H-bond Donor	-	0.475
H-bond Acceptor	-	-

^{u} after the leave-one-out method, the correlation coefficient was cross-validated; ^{V} coefficient of correlation not cross-validated; ^{W} The estimate standard error; ^{x} test result F; ^{y} For test set predictions, the correlation coefficient; ^{z} Optimum number of components.

The statistical parameters of the model CoMFA, the cross-validated Q^2 value according to the (LOO) analysis, is 0.625 with nine components; the traditional $R^2 = 0.996, F = 622.370$ and the standard error of estimated $SEE = 0.043$ are the results of the non-cross-validated PLS analysis. Electrostatic descriptors only account for 40% of the variance, with steric field descriptors accounting for 60%. The graph below represents the correlation between the experimental and predicted activity, which completes the statistical results obtained in the CoMFA model, as seen in Figure 2.

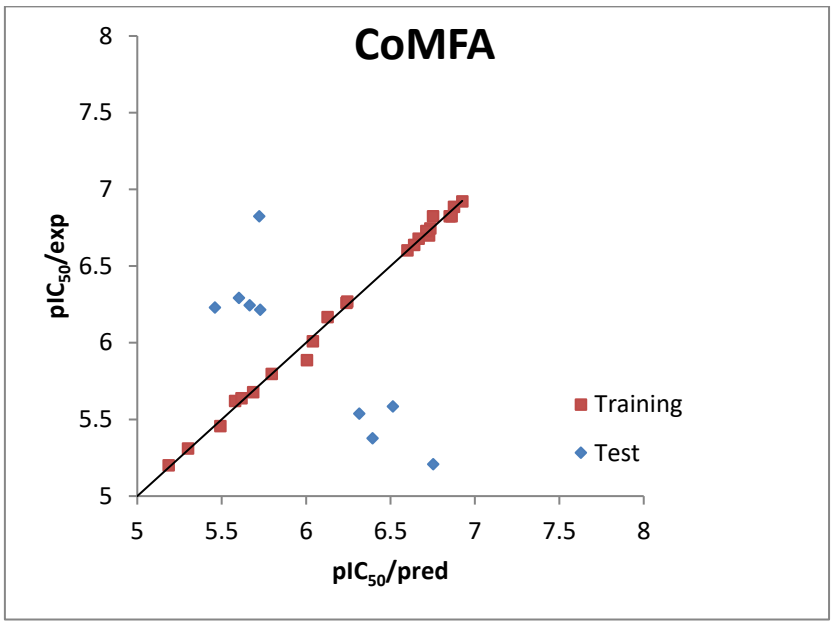

Figure 2. The relationship between the activities that were predicted and those that were experimental.

To find the optimal CoMSIA model, some potential combinations of various fields were tested; the combination of hydrophobic, steric, and H-bond donor fields with nine components produced the best cross-validated model (Q^2= 0.631, R^2= 0.738, F= 59.122, SEE = 0.298). Comparable contributions from the steric (S), hydrophobic (H), and H-bond donor (HBD) fields showed percentages of 25.4%, 27.1%, and 47.5%, respectively; these results indicate the interesting role of the H-bond donor fields in the activity studied. The relationship between the experimental and predicted pIC_{50} values presented in Figures 2 and 3 show that the CoMFA model has a higher correlation than CoMSIA. Therefore, the CoMFA model has a better predictive ability than the CoMSIA model, as shown by the cross-validation results, which proves the choice of the CoMFA model. The graph below represents the correlation between the experimental and predicted activity, completing the statistical results obtained in the CoMSIA model, as seen in Figure 3.

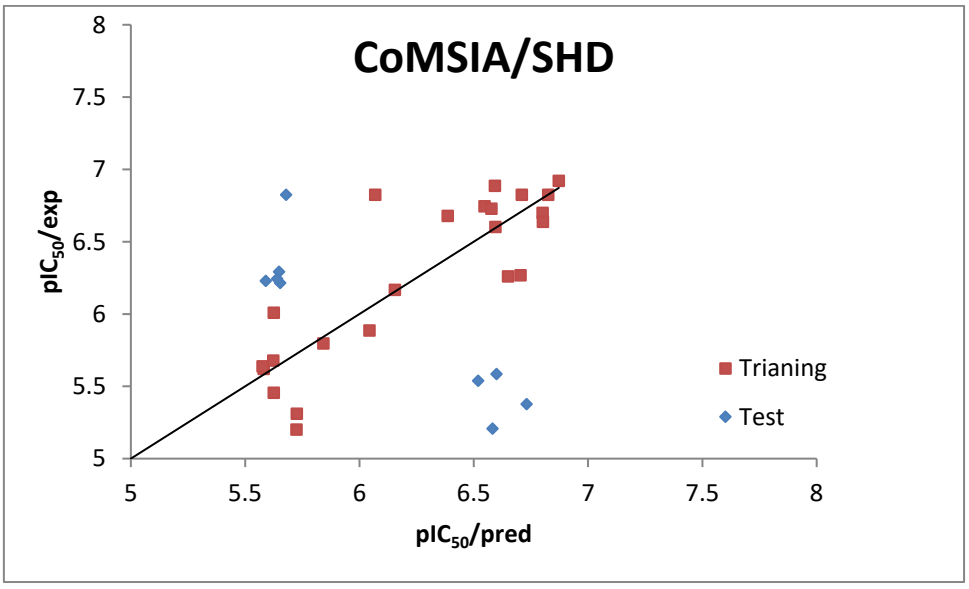

Figure 3. The relationship between the activities that were predicted and those that were experimental.

According to the findings of these techniques, the CoMFA and CoMSIA models will be accurate when applied to forecast how new HIV-1 entry inhibitors will behave. They also

show that these models have a higher capacity for incorporating new data than the CoMSIA model; the CoMFA model offers a high predictive R^2 and SEE while requiring fewer residual values from the test set.

3.2. CoMFA contour map analysis.

The Comparative Molecular Field Analysis (CoMFA) technique was employed to analyze the steric and electrostatic interactions within a molecular system. These interactions are crucial for understanding how molecules interact with their surroundings, such as in biological or chemical processes. The CoMFA maps provide a visual representation of these interactions, with distinct colors highlighting favorable and unfavorable regions. The CoMFA maps of the most active molecule (N°31) are presented in Figure 4.

The yellow and green, which are sterically unfavorable and sterically favorable, respectively, contours viewed at the CoMFA contour map level (figure. 4(A).) indicate 20% and 80% of the participation, respectively. Similar to this, in the CoMFA electrostatic area, the blue (favorable electropositive charge) and red (favorable electronegative charge) contours account for 80% and 20% of the participation, respectively (figure. 4(B)). The bulky group in this area is critical for the inhibitory effect, according to the sterically advantageous green outlines in substituents. R_5, R_8, and R_9, respectively. Based on the structure and activity of compound 31 (($R_5 = H$,$R_8 = CH_3$ and $R_9 = CH_3$), $pIC_{50} = 6.921$), it can be seen that the insertion of the bulky substituents R_5, R_8 and R_9 increases inhibitory activity, the green outline may give a reason why the functioning of compounds 5,6,7,8,18, and 19 which have the substituents ($R_5 = H$, $R_8 = H$ and $R_9 = H$) are less inhibiting than compound 31. The figure. 4(A) shows two favorable steric yellow contours can be seen, one around the methoxy group of compounds 31 and the other around the halogen. Red areas surrounded by amide groups can be seen in the electrostatic contour plot of CoMFA. This suggests that electronegative groups' occupation of this region is favorable for the suppressive effects of HIV-1 entry inhibitors. On the other hand, Rings of pyrrole and benzene-containing halogens encircle the mid-blue contour map. The electropositive substituents in these blue regions are causing a rise in activity, as indicated by the color.

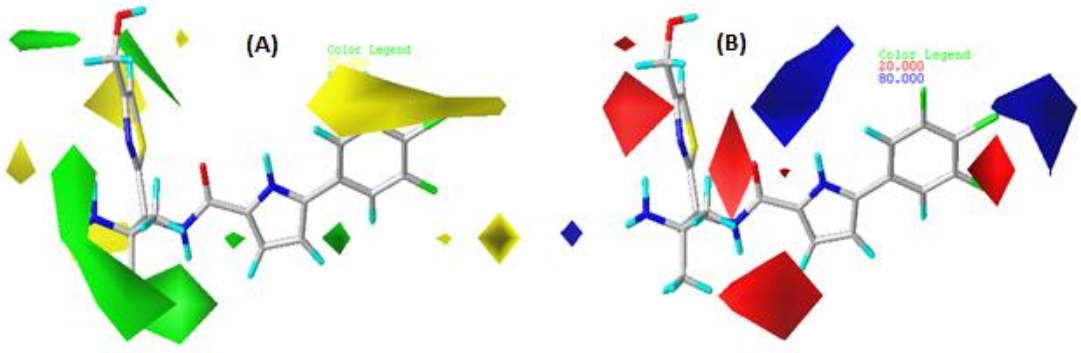

Figure 4. Using compound 31 to create CoMFA contour maps. **(A)** The green (sterically favorable) and yellow (sterically unfavorable); **(B)** the blue (favorable electropositive charge) and red (favorable electronegative charge).

3.3. CoMSIA contour map analysis.

CoMSIA (SHD) proved to be the best among all other field combinations and predicted good statistical results. Contour plots are created based on this model. The spatial and electrostatic contour plots of CoMSIA are shown in Figures 5 (A) and (B), which show similar trends to

those of CoMFA. Therefore, this result also confirms the CoMFA contour maps and their interpretation. The hydrophobicity contour plot of CoMSIA is shown in Figure 5(C).

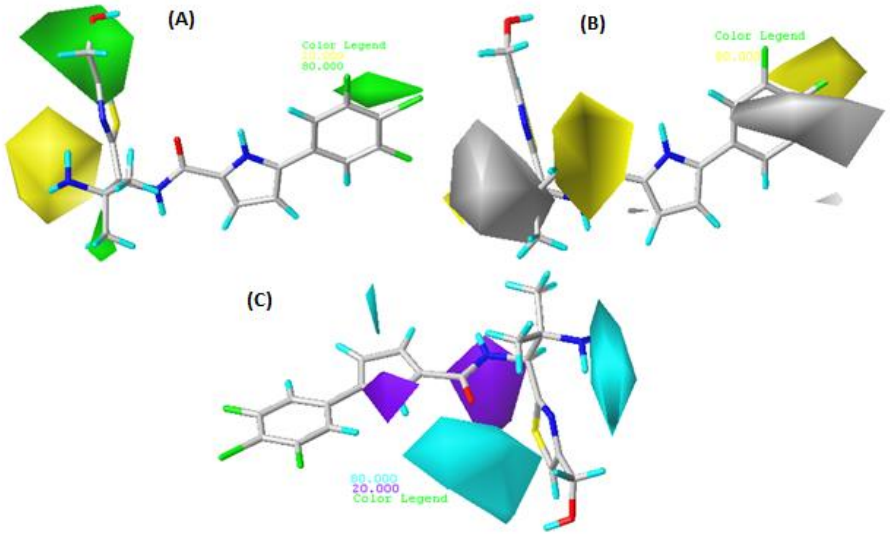

Figure 5. Using compound 31, create CoMSIA contour maps. **(A)** The green (sterically favorable) and yellow (sterically unfavorable); **(B)** The yellow (hydrophobic favorable) and white (hydrophilic unfavorable); **(C)** hydrogen donor bonds.

The zones with the most advantageous alterations, which boost the HIV-1 entry inhibitors, are shown green sterically favorable in Figure 5(A) as the contour map contribution is 80%, and the favorable locations are highlighted in yellow with a 20% contribution. Figure 5(B) demonstrates the CoMSIA model hydrophobic contour map. The outlines of white (hydrophilic favorable) and yellow (hydrophobic favorable) of the CoMSIA hydrophobic field. The hydrophobic groups in this region are chosen for HIV-1 entrance inhibitors as indicated by the polyhedron in yellow surrounding the halogen atom on the benzene ring, and the amide groups, respectively, have a lower potency than compounds 31 ($R_2 = cl$ and $R_2 = F$, $pIC_{50} = 6.921$), and the same is true for the white contours hydrophilic. Figure 5(C) shows the contours of the hydrogen bonding donor fields such that the cyan color shows the favorable regions (80% contribution), and the purple color shows the unfavorable regions (20% contribution).
We observe a cyan outline close to the amine and sulfur. Hydrogen donor bonds increase the activity, and the underdeveloped area is indicated by the purple contours of the underprivileged area. These interactions are in addition to the interactions of the hydrogen bond donor modeled from CoMSIA field interactions. In conclusion, maps with contours provided by the CoMFA and CoMSIA have enough information based on the findings of the 3D-QSAR studies conducted in this work to enable us to comprehend the structures of the compounds and their inhibitory effects by 3D-QSAR. Further altering the benzene ring and the methyl groups of this chemical, considering steric, electrostatic, and hydrophobic properties, further compounds with the necessary inhibitory action may be created.
After completion, 3 D- QSAR contour maps were generated to visualize the contour of the CoMFA and CoMSIA model data, which provide information about the favorable and unfavorable regions for biological activity in the studied compounds. Changes in the molecule's structure lead to changes in the physicochemical properties, which could increase or decrease the biological activity. We have summarized most of this work in the sterile, electrostatic, hydrophobic, and hydrogen bond donors contour maps, as shown in Figure 6. Compound 31 is the most active, so it was taken as the reference structure for generating the contour maps.

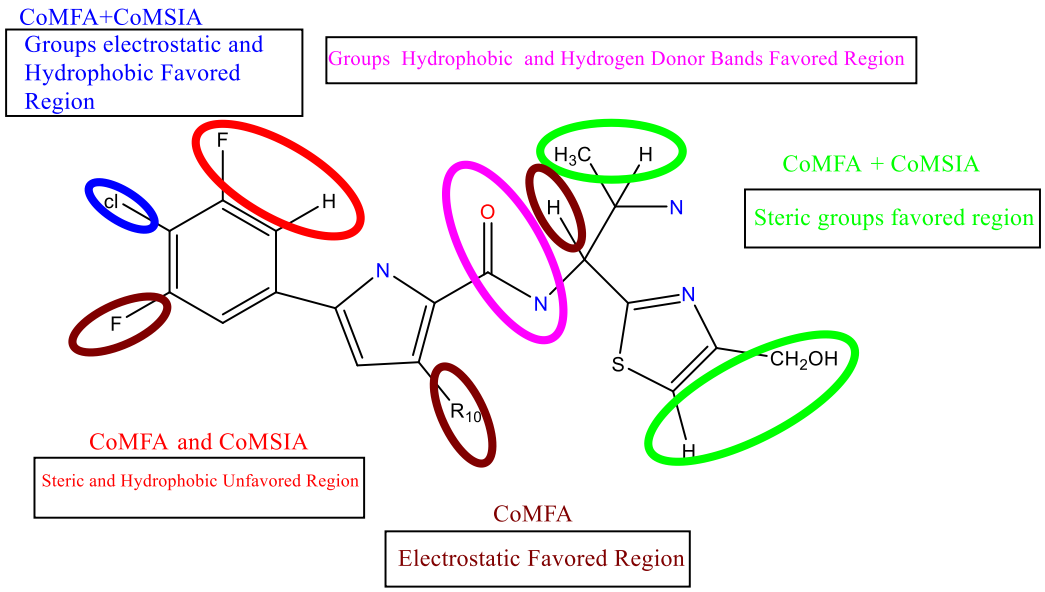

Figure 6. Summary of the structure-activity relationship determined from the CoMFA and CoMSIA models.

4. Conclusions

Utilizing the CoMFA and CoMSIA tools, the 3D-QSAR research of 32 HIV-1 entry inhibitors was conducted for statistical analysis of the Q^2 values of CoMFA (Q^2= 0.625, R^2=0.996) and CoMSIA (Q^2= 0.631, R^2= 0.738) meet the requirements. The accepted statistical validity criteria (Q^2> 0.5) permit the supposition of an important QSAR. Every model created has demonstrated statistical significance and predictive powers. According to the cross-validation results, the CoMFA exemplary is thought to be more predictive compared to the CoMSIA model; it has a strong correlation with the findings of additional tests, which makes the model be validated. The contour maps for CoMFA and CoMSIA provide a thorough picture of the development of novel inhibitors in the medical field. Using the maps contours CoMSIA and CoMFA, novel inhibitors with improved inhibitory activity can be created.

Funding

This research received no external funding.

Acknowledgments

The authors would like to thank the anonymous reviewers for their valuable comments and suggestions on improving the paper's quality.

Conflicts of Interest

We wish to confirm that there are no known conflicts of interest associated with this publication, and there has been no significant financial support for this work that could have influenced its outcome.

References

1. Prévost, J.; Tolbert, W.D.; Medjahed, H.; Sherburn, R.T.; Madani, N.; Zoubchenok, D.; Gendron-Lepage, G.; Gaffney, A.E.; Grenier, M.C.; Kirk, S.; Vergara, N.; Han, C.; Mann, B.T.; Chénine, A.L.; Ahmed, A.; Chaiken, I.; Kirchhoff, F.; Hahn, B.H.; Haim, H.; Abrams, C.F.; Smith III, A.B.;Sodroski, J.; Pazgier, M.;

Finzi, A. The HIV-1 Env gp120 Inner Domain Shapes the Phe43 Cavity and the CD4 Binding Site. *MBio* **2020**, *11*, 10-1128, https://doi.org/10.1128/mBio.00280-20.
2. Chen, B. Molecular Mechanism of HIV-1 Entry. *Trends Microbiol.* **2019**, *27*, 878-891, https://doi.org/10.1016/j.tim.2019.06.002.
3. Gumel, S.D.; Ibrahim, A.; Olayinka, A.T.; Ibrahim, M.S.; Balogun, M.S.; Dahiru, A.; Ajayi, I.; Ajumobi, O.; Ahmadu, I.; Song, A.; Maifada, A.I.; Abdullahi, H. HIV-Malaria co-infection and its determinants among patients attending antiretroviral treatment clinic in Zaria Kaduna state Nigeria. *J Interval Epidemiol Public Health.* **2021**, *4*, 2, https://doi.org/10.37432/jieph.2021.4.1.31.
4. Mayer, K.H.; Allan-Blitz, L.T. Similar, but different: drivers of the disproportionate HIV and sexually transmitted infection burden of key populations. *J. Int. AIDS Soc.* **2019**, *22*, e25344, https://doi.org/10.1002/jia2.25344.
5. Gupta, P.K.; Saxena, A. HIV/AIDS: Current Updates on the Disease, Treatment and Prevention. *Proc. Natl. Acad. Sci., India, Sect. B Biol. Sci.* **2021**, *91*, 495–510, https://doi.org/10.1007/s40011-021-01237-y.
6. Saag, M.S.; Gandhi, R.T.; Hoy, J.F.; Landovitz, R.J.; Thompson, M.A.; Sax, P.E.; Smith, D.V.; Benson, C.A.; Buchbinder, S.P.; Del Rio, C.; Eron Jr., J.J.; Fätkenheuer, G.; Günthard, H.F.; Molina, J.M.; Jacobsen, D.M.; Volberding, P.A. Antiretroviral Drugs for Treatment and Prevention of HIV Infection in Adults: 2020 Recommendations of the International Antiviral Society-USA Panel. *J. Am. Med. Assoc.* **2020**, *324*, 1651–1669, https://doi.org/10.1001/jama.2020.17025.
7. Brandt, C.P.; Paulus, D.J.; Lopez-Gamundi, P.; Green, C.; Lemaire, C.; Zvolensky, M.J. HIV Anxiety Reduction/Management Program (HAMRT): pilot randomized controlled trial. *Psychol. Socio-Med. Asp. AIDS/HIV* **2019**, *31*, 1527–1532, https://doi.org/10.1080/09540121.2019.1597962.
8. Vanhamel, J.; Bruggemans, A.; Debyser, Z. Establishment of latent HIV-1 reservoirs: what do we really know?. *J. Virus Erad.* **2019**, *5*, 3–9, https://doi.org/10.1016/s2055-6640(20)30275-2.
9. Ramos-Martín, F.; D'Amelio, N. Drug Resistance: An Incessant Fight against Evolutionary Strategies of Survival. *Microbiol. Res.* **2023**, *14*, 507-542, https://doi.org/10.3390/microbiolres14020037.
10. Temereanca, A.; Ruta, S. Strategies to overcome HIV drug resistance-current and future perspectives. *Front. Microbiol.* **2023**, *14*, 342, https://doi.org/10.3389/fmicb.2023.1133407.
11. Moranguinho, I.; Taveira, N.; Bártolo, I. Antiretroviral Treatment of HIV-2 Infection: Available Drugs, Resistance Pathways, and Promising New Compounds. *Int. J. Mol. Sci.* **2023**, *24*, 5905, https://doi.org/10.3390/ijms24065905.
12. Rullo, E.V.; Ceccarelli, M.; Condorelli, F.; Facciolà, A.; Visalli, G.; D'Aleo, F.; Paolucci, I.; Cacopardo, B.; Pinzone, M.R.; Di Rosa, M.; Nunnari, G.; Pellicanò, G.F. Investigational drugs in HIV: Pros and cons of entry and fusion inhibitors. *Mol. Med. Rep.* **2019**, *19*,1987–1995, https://doi.org/10.3892/mmr.2019.9840.
13. Ratcliff, A.N.; Venner, C.M.; Olabode, A.S.; Knapp, J.; Pankrac, J.; Derecichei, I.; Gibson, R.M.; Finzi, A.; Li, Y.; Mann, J.F.S.; Arts, E.J. Enhancement of CD4 Binding, Host Cell Entry and Sensitivity to CD4bs Antibody Inhibition Conferred by a Natural but Rare Polymorphism in the HIV-1 Envelope. *J. Virol.* **2022**, *96*, e01851-21, https://doi.org/10.1128/jvi.01851-21.
14. Jiang, C.; Huang, H.; Kang, Z.; Yang, L.; Xi, Z.; Sun, H.; Pluth, M.D.; Yi, L. NBD-based synthetic probes for sensing small molecules and proteins: design, sensing mechanisms and biological applications. *Chem. Soc. Rev.* **2021**, *50*, 7436–7495, https://doi.org/10.1039/d0cs01096k.
15. De Almeida, R.F.M.; Santos, T.C.B.; da Silva, L.C.; Suchodolski, J.; Krasowska, A.; Stokowa-Sołtys, K.; Puchalska, M.; Starosta, R. NBD derived diphenyl(aminomethyl)phosphane – A new fluorescent dye for imaging of low pH regions and lipid membranes in living cells. *Dyes Pigm.* **2021**, *184*, 108771, https://doi.org/10.1016/j.dyepig.2020.108771.
16. Dutta, T.; Pal, K.; Koner A.L. Cellular metabolic activity marker via selective turn-ON detection of transporter protein using nitrobenzoxadiazole-based fluorescent reporter. *Sci. Rep.* **2020**, *10*, 4166, https://doi.org/10.1038/s41598-020-60954-y.
17. El Masaoudy, Y.; Tabti, K.; Koubi, Y.; Maghat, H.; Lakhlifi, T.; Bouachrine, M. In silico design of new pyrimidine-2,4-dione derivatives as promising inhibitors for HIV Reverse Transcriptase-associated RNase H using 2D-QSAR modeling and (ADME/Tox) properties. *Mor. J. Chem.* **2023**, *11*, 11-12, https://doi.org/10.48317/IMIST.PRSM/morjchem-v11i2.35455.
18. Tabti, K.; El mchichi, L.; Sbai, A.; Maghat, H.; Bouachrine, M.; Lakhlifi, T. 2D AND 3D-QSAR/COMSIA COMPARATIVE STUDY ON A SERIES OF THIAZOLE DERIVATIVES AS SDHI INHIBITORS. *Maghrebian J. Pure Appl. Sci.* **2020**, *6*, 73–90, https://doi.org/10.48383/IMIST.PRSM/mjpas-v6i2.23108.

19. Tabti, K.; Hajji, H.; Sbai, A.; Maghat, H.; Bouachrine, M.; lakhlifi, T. Identification of a Potential Thiazole Inhibitor Against Biofilms by 3D QSAR, Molecular Docking, DFT Analysis, MM-PBSA Binding Energy Calculations, and Molecular Dynamics Simulation. *Phys. Chem. Res.* **2023**, *11*, 369–389.
20. Curreli, F.; Ahmed, S.; Victor, S.M.B., Iusupov, I.R.; Spiridonov, E.A.; Belov, D.S.; Altieri, A.; Kurkin, A.V.; Debnath, A. K. Design, synthesis, and antiviral activity of a series of CD4-mimetic small-molecule HIV-1 entry inhibitors. *Bioorg. Med. Chem.* **2021**, *32*, 116000, https://doi.org/10.1016/j.bmc.2021.116000.
21. El fadili, M.; Er-rajy, M.; Imtara, H.; Kara, M.; Zarougui, S.; Altwaijry, N.; Al kamaly, O.; Al Sfouk, A.; Elhallaoui, M. 3D-QSAR, ADME-Tox In Silico Prediction and Molecular Docking Studies for Modeling the Analgesic Activity against Neuropathic Pain of Novel NR2B-Selective NMDA Receptor Antagonists. *Processes* **2022**, *10*,1462, https://doi.org/10.3390/pr10081462.
22. Deng, Y.t.; Wang, J.-w.; Chu, H.; Wang, J.; Hu, Y.; Iin, Y.; Shu, M.; Lin, Z.-h. 3D-QSAR and Docking Studies on Pyrimidine Derivatives as CSF-1R Inhibitors. *Lett. Drug Des. Discov*. **2020**, *17*, 341–355, https://doi.org/10.2174/1570180816666190329224946.
23. Salman, H.A.; Yaakop, A.S.; Aladaileh, S.; Mustafa, M.; Gharaibeh, M.; Kahar, U.M. Inhibitory effects of *Ephedra alte* on IL-6, hybrid TLR4, TNF-α, IL-1β, and extracted TLR4 receptors: in silico molecular docking. *Heliyon* **2023**, *9*, e12730, https://doi.org/10.1016/j.heliyon.2022.e12730.
24. Gao, Y.; Wang, H.; Wang, J.; Cheng, M. In silico studies on p21-activated kinase 4 inhibitors: comprehensive application of 3D-QSAR analysis, molecular docking, molecular dynamics simulations, and MM-GBSA calculation. *J. Biomol. Struct. Dyn*. **2020**, *38*, 4119–4133, https://doi.org/10.1080/07391102.2019.1673823.
25. Mancilla, Y.; Mendoza, A. Application of partial least squares as a complementary and preliminary receptor model for source apportionment of ambient aerosol based on molecular organic markers. *J. Chemom*. **2019**, *33*, e3136, https://doi.org/10.1002/cem.3136.
26. Lian, Z.; Sang, C.; Li, N.; Zhai, H.; Bai, W. 3D,2D-QSAR study and docking of novel quinazolines as potential target drugs for osteosarcoma. *Front. Pharmacol*. **2023**, *14*, 1124895, https://doi.org/10.3389/fphar.2023.1124895.
27. Salimi, A.; Lim, J.H.; Jang, J.H.; Lee, J.Y. The use of machine learning modeling, virtual screening, molecular docking, and molecular dynamics simulations to identify potential VEGFR2 kinase inhibitors. *Sci. Rep.* **2022**, *12*, 18825, https://doi.org/10.1038/s41598-022-22992-6.
28. Vishwakarma, K.; Bhatt, H. Molecular modelling of quinoline derivatives as telomerase inhibitors through 3D-QSAR, molecular dynamics simulation, and molecular docking techniques. *J. Mol. Model.* **2021**, *27*, 30, https://doi.org/10.1007/s00894-020-04648-2.
29. Zhu, J.; Jia, L.; Jiang, Y.; Yu, Q.; Xu, L.; Cai, Y.; Chen, Y.; Li, H.; Gang, H.; Liang, W.; Jin, J. Integrated molecular modeling techniques to reveal selective mechanisms of inhibitors to PI3Kδ with marketed Idelalisib. *Chem. Biol. Drug Des.* **2021**, *97*, 1158–1169, https://doi.org/10.1111/cbdd.13838.
30. Parkali, P.M.; Kumar, A.S.; Johanna, P.K.; Prodensia, T.S.; Turaga, S.; Shaiva, V.; Pujar, G.V.; Joshi, S.D.; Aminabhavi, T.M.; Dixit, S.R. Molecular Docking and Three-Dimensional Quantitative Structure–Activity Relationships for Antitubercular Pyrimidine Derivatives. *Polycycl. Aromat. Compd.* **2022**, *42*, 4132–4145, https://doi.org/10.1080/10406638.2021.1885455.